Article | Received 5 July 2024; Accepted 20 August 2024; Published 28 August 2024
https://doi.org/10.55092/rse20240007

High-strength polyvinyl alcohol/epoxy-functionalized gallic acid dual-crosslinked binder for silicon anodes

Junchao Sun[1,†], Jing Jiang[1,†], Zhengshuai Xu[1], Lintianfang Su[1], Yongyin Cui[2,*], Hongwei Pan[3,*] and Lan Cao[1,*]

[1] Key Laboratory of Advanced Rubber Material, Ministry of Education, Qingdao University of Science and Technology, Qingdao 266042, China
[2] Weihai Marine Organism & Medical Technology Research Institute, College of Marine Science and Technology, Harbin Institute of Technology, Weihai 264209, China
[3] Department of materials Science (MTM), KU Leuven, Leuven 3001, Belgium
[†] These authors contributed equally to this work.

* Correspondence authors; E-mails: 23b330003@stu.hit.edu.cn (Y.C.); hongwei.pan@kuleuven.be (H.P.); lancao@qust.edu.cn (L.C.).

Abstract: Silicon is increasingly recognized as a promising candidate for the next generation of high-capacity anodes in lithium-ion batteries. However, its substantial volumetric changes during charge and discharge cycles significantly reduce battery lifespan, which hampers its further development and practical application. Developing novel binders represents a critical strategy to overcome these challenges. PG (modified gallic acid crosslinked polyvinyl alcohol) exhibited excellent adhesion (1.28 N) and mechanical strength (89 MPa). Moreover, at a current density of 420 mA g^{-1}, the PG55 (polyvinyl alcohol: modified gallic acid = 50:50 wt %) electrode maintained an impressive specific capacity of 2480 mAh g^{-1} after 100 cycles. Further increasing the current density to 840 mA g^{-1}, the PG55 electrode retained a capacity of 1822 mAh g^{-1} after 200 cycles, while maintaining high coulombic efficiency throughout the cycling process. This study provides a significant reference for the ongoing evolution of binders applied for silicon anode.

Keywords: Si anode; dual-crosslinked network binder; stable cycling

1. Introduction

With the rapid development of new energy vehicles and large-scale integrated circuits, lithium-ion batteries (LIBs) are playing an increasingly important role [1–3]. The anode, as a crucial component of LIBs, has a decisive impact on the capacity and energy density of the batteries [4–6]. Currently, almost all commercial LIBs use graphite as the anode material, which has a theoretical specific capacity of only 372 mAh g^{-1} [7]. Despite continuous research, the performance of graphite anodes in practical applications has nearly reached its

theoretical limit, failing to meet the growing energy demands [8]. Silicon, the second most abundant element in the Earth's crust, offers a low lithium intercalation potential and an ultra-high theoretical specific capacity of 4200 mAh·g^{-1} at high temperatures and pressures, with a theoretical capacity of 3579 mAh·g^{-1} under ambient conditions [9]. However, during the cyclic lithiation/delithiation process, silicon undergoes significant volume changes (>300%), leading to particle fracture, pulverization, and even electrode structure damage and detachment, severely affecting the battery's cycling stability [9,10]. Furthermore, continuous volume changes can disrupt the solid electrolyte interphase (SEI) formed on the anode surface, resulting in repeated decomposition reactions of the electrolyte, accelerating electrolyte loss, and shortening the battery's cycle life [11–13]. These challenges have significantly limited the further development of silicon anodes.

In recent years, various approaches have emerged to tackle the challenges associated with silicon anodes. These include the synthesis of silicon nanomaterials, the advancement of porous silicon structures, the utilization of silicon-carbon composites, and the engineering of artificial SEI films on silicon anode surfaces [14–17]. However, these strategies face obstacles in commercialization due to their intricate processes and high expenses. Conversely, the development of innovative polymer binders presents a viable solution. These binders can seamlessly integrate into established electrode fabrication procedures, offering simplified manufacturing and reduced costs, thus showcasing the substantial potential for commercial viability [18–20]. Consequently, the quest for polymer binders tailored for silicon anodes has progressively become a pivotal area of research.

Research indicates that polymer binders suitable for silicon anodes typically possess specific characteristics. Primarily, the functional groups within the polymer binder should interact with silicon particles to anchor them, with hydrogen bonding and van der Waals forces being the most prevalent interactions [18,21]. Polymers such as polyacrylic acid (PAA) [22,23], carboxymethyl cellulose (CMC) [24,25], polyvinyl alcohol (PVA) [26,27], and natural polysaccharides fulfill these criteria. However, the weak interactions between silicon and the binder are insufficient to counteract the mechanical stress caused by silicon volume expansion [21]. Therefore, strong intermolecular interactions are also necessary between the polymer binder chains [28,29]. For example, Jeong *et al.* introduced the concept of "dynamic crosslinking" for silicon nanoparticle anodes by utilizing host-guest interactions between supermolecular crosslinkers comprising hyperbranched β-cyclodextrin polymer (β-CDp) and a dendritic sebacic acid derivative containing six adamantane units. This supermolecular network endowed the binder with self-healing properties, preserving electrode structure integrity and improving electrode cycling stability amid silicon's continuous volume changes [30]. To further enhance the cycling stability of silicon anodes, our prior work investigated water-based dual crosslinked network binders featuring both hydrogen and covalent bonds. Specifically, a dual crosslinked network binder, PE, was fabricated using epoxidized natural rubber and aminated polyacrylic acid. This binder exhibited reversible deformability and sufficient mechanical strength, with numerous active groups in its molecular chains ensuring strong adhesion between the active material and the current collector. It effectively mitigated and adjusted to the volume changes of silicon

anodes, resulting in a stable interface and a cycling-stable silicon anode [31]. At the same time, some functional binders have also attracted wide attention [32–34]. For example, Jin *et al.* developed a self-healing polyelectrolyte binder by in-situ crosslinking polydopamine, phytic acid and poly (acrylamide-2- (dimethylamino) ethyl acrylate) [35].

Combining the discussions above, in this study, we modified gallic acid (GA) with epichlorohydrin (ECH) and blended it with polyvinyl alcohol (PVA) to create a binder featuring a dual-crosslinked three-dimensional network structure with a dual network structure of hydrogen bonds and covalent bonds. Notably, the PG55 binder demonstrated outstanding overall performance. As shown in Scheme 1, in this binder system, the ECH-modified GA introduced epoxy functional groups into its side chains, providing active sites for further covalent crosslinking with the hydroxyl groups in PVA. The red line represents the interface between the active material Si and the binder. Moreover, polyvinyl alcohol possessed numerous hydroxyl groups on its main chain, capable of forming hydrogen bonds with oxygen-containing functional groups on the surface of silicon and the current collector, as well as with active groups such as esters and hydroxyls in ECH-modified GA (ECH-GA), thereby ensuring strong bonding between the active material and the current collector, and effective anchoring of the Si active material. The binder's dual-network structure incorporated both "static" (chemical crosslinking) and "dynamic" (physical crosslinking) interactions, offering abundant crosslinking points to disperse and transfer the stress generated by silicon anode expansion during cycling. This effectively suppressed silicon volume changes, thereby preserving electrode structure integrity, extending battery life, and providing a straightforward and efficient solution for developing novel binders for silicon anodes.

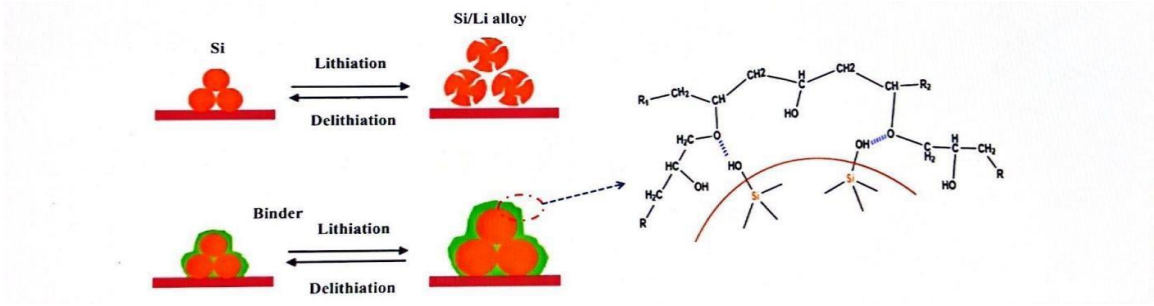

Scheme 1. The working mechanism of PG binders applied to silicon anodes.

2. Methods and materials

Materials: Silicon nanoparticles (average particle size 50–100 nm) were purchased from Shenzhen Youyan Platform, conductive carbon black (Super P) was purchased from Shenzhen Youyan Platform, poly(vinyl alcohol) (PVA, alcoholysis degree 87%–89%) was from Shanghai McLean Company Limited, epichlorohydrin (ECH) was purchased from Sinopharm Group Chemical Reagent Company Limited, chitosan (CS) was purchased from Shanghai Aladdin Company Limited, sodium hydroxide (NaOH) was purchased from Sinopharm Group Chemical Reagent Company Limited.

Preparation of GA-ECH: 1 g GA was dissolved in 50 mL water and stirred continuously during the process of heating to 100 ℃; after GA was completely dissolved, the solution was cooled down to 50 ℃, then ECH was added by the molar ratio of 1:10 (GA: ECH), then 0.1 g of 1% tetrabutylammonium iodide (TBAI) was added as the catalyst, and the reaction was opened for 5 h, and then sodium hydroxide was added 10ml concentration of 2% dropwise after the solution was cooled down to room temperature and the reaction was closed for 2 h. After the reaction, the excess ECH was removed by a rotary evaporator and finally freeze-dried for 24 h to obtain modified gallic acid (GA-ECH).

Preparation of PVA/GA-ECH crosslinked film: PVA and modified GA were compounded according to the mass ratio of 7:3, 5:5, 3:7, and a small amount of tertiary amine alkaline substance was added as a catalyst, stirred well, and then poured into the molds, and finally was dried in a vacuum oven at 100 ℃ for 8 h. The prepared adhesive films were named as PG73, PG55, and PG37, respectively.

Preparation of Si anode: A mixture of silicon powder and Super P in a 6:2 ratio was combined with a PVA solution and stirred for 2 h to create a homogeneous slurry. Then, GA-ECH and a drop of TBAI catalyst were added and stirred for an additional 5 h, resulting in a final ratio of silicon powder, Super P, and binder of 6:2:2. The slurry was then coated onto a copper foil using a spatula and placed in a vacuum drying oven for 12 h. Afterward, the coated material was cut into pieces, weighed, and returned to the vacuum-drying oven for another 12 h. The final mass loading of silicon is 1.53 mg, and the areal density is 1.0 mg cm^{-2}.

Assembling of button half cell: The prepared pole pieces were assembled into a CR2032 cell in a glove box filled with inert gas, using lithium as the reference electrode; Celgard 2500 diaphragm was used, and the electrolyte was 1 M $LiPF_6$ dissolved in ethylene carbonate (EC), diethyl ethyl carbonate (DEC), and ethyl methyl carbonate (EMC) in the volume ratio of 1:1:1, and 10% fluorine-substituted ethylene carbonate (FEC) was added to it, and the electrolyte volume was 120 μL.

Material characterization: FTIR spectra were tested on samples that were scanned using a Bruker VERTEX-70 (Karlsruhe, Germany) with a resolution of 4 cm^{-1} and a scanning range of 600–4000 cm^{-1}. ^{1}H-HMR was measured using a Bruker Avance 400 Nuclear Magnetic Resonance Spectrometer (Karlsruhe, Germany). XRD was tested by a TESCAN MIRA (Toshima, Tokyo) using Cu Kα radiation (λ = 0.154 nm) was tested. Differential Scanning Calorimetry (DSC) was tested on a DSC manufactured by DSC204F1S Ray Diffractometer, (Selb, Germany). Tensile and 180 °peeling experiments were performed on the samples using an electronic tensile tester (Zwick/Roell Z005, Ulm, Germany). In the tensile test, the samples (50 mm × 5 mm) were tested at a tensile rate of 5 mm min^{-1}. In the 180 ° peeling test, the prepared poles were first cut into rectangles of 30 cm in length and 15 cm in width and then peeled off at a tensile rate of 10 mm min^{-1} by using a 10 cm wide piece of 3M adhesive tape to adhere to the side coated with the active material. Nanoindentation was performed with a Berkovich nanoindentation tester (Nano Test Vantage, Wrexham, Wales, England). The swelling test can show the stability and absorption characteristics of the adhesive in the electrolyte, and the swelling was calculated according to the following formula: swelling rate = 100% × $(m_b - m_a)/m_a$, where m_a and m_b are the mass of the electrode

before and after swelling, respectively. SEM was performed using a TESCAN MIRA, which was used to observe the surface and cross-section morphology of the samples.

Electrochemical characterization: charge/discharge tests and multiplicative charge/discharge were performed on the cells at 0.005–1.5 V using the Blue Power System. Cyclic voltammetric tests were performed on the cells using a Bio-Logic electrochemical workstation with 5 and 3 scans at 0.001–1.5 V using a voltage scan rate of 0.1 mV s^{-1}. EIS tests were performed on a Bio-Logic VMP3 electrochemical workstation with a scanning interval of 100 mHz-7 MHz and an amplitude of 5 mV. All potentials in this paper are based on (vs. Li/Li^+), and all tests were performed at room temperature (~30 ℃).

3. Results and discussion

To confirm the success of the epoxy functionalization of GA (Figure 1a) and its subsequent cross-linking reaction (Figure 1b), we conducted detailed structural characterization using ^1H NMR and FTIR. First, as shown in the ^1H NMR spectrum in Figure 1c, the peak at 3.3 ppm corresponds to water. The proton absorption peaks of the epoxy group in ECH are located at 2.6 ppm and 2.8 ppm, and the peaks for -CH_2- appear at 3.5–3.9 ppm. For GA, the proton absorption peaks on the benzene ring are at6.91 ppm, and the characteristic peaks of the phenolic hydroxyl groups are 8.7–9.4 ppm. After modification with ECH, GA shows proton peaks of the epoxy group at 2.6–2.9 ppm and characteristic peaks of -CH_2- at 3.5–3.9 ppm. Due to changes in the substituents on the benzene ring, the proton absorption peaks on the benzene ring shift to 7.12 ppm. As seen in the FTIR spectrum in Figure 1d, the peaks in the GA spectrum at 3492 cm^{-1}, 3274 cm^{-1}, and 1660 cm^{-1} correspond to the -OH groups on the benzene ring, the -OH in carboxylic acids, and the -C=O group in benzoic acid, respectively. The peaks at 1602 cm^{-1} and 858 cm^{-1} represent the C=C absorption peaks in the benzene ring. After modification with ECH, the -OH peak on the benzene ring disappears and transforms into the -OH peak in the alkyl group (3481 cm^{-1}). Additionally, characteristic peaks of the epoxy group and -CH_2- appear at 912 cm^{-1}, 2943 cm^{-1}, and 2885 cm^{-1}. These results collectively confirm the successful epoxy modification of GA. Finally, after cross-linking GA with polyvinyl alcohol, the epoxy group peak at 912 cm^{-1} disappears, the ether bond peaks 1000–1300 cm^{-1} significantly increase, and the -OH peaks generated by the ring-opening reaction are noticeably strengthened, showing a shift due to hydrogen bonding. These results indicate that GA has successfully cross-linked with polyvinyl alcohol, and hydrogen bonds have formed between them.

Mechanical properties are essential for evaluating an adhesive's ability to accommodate the volume changes of silicon anodes. Superior mechanical performance is crucial for maintaining the structural integrity of electrodes and ensuring interfacial stability [36]. Figure 2a displays the tensile curves of various films, showing that the PVA film exhibits a mechanical strength of 46 MPa and an elongation at break of 122%. When PVA is cross-linked with GA-ECH, the film's elongation at break decreases sharply with an increase in GA-ECH content, while its mechanical strength increases rapidly. Notably, the tensile strengths of the PG73, PG55, and PG37 adhesive films reach 61 MPa, 89 MPa, and 126 MPa, respectively,

all demonstrating high mechanical strength. This significant enhancement in mechanical properties enables these adhesive films to effectively suppress the volume changes of silicon particles, preventing the fracture and pulverization of silicon during charge and discharge cycles. High mechanical strength not only helps maintain the structural integrity of the electrode but also ensures the stability of the electrode-electrolyte interface during cycling, thereby extending the battery's lifespan [37]. Additionally, the mechanical performance of the films is critical for the reliability and stability of the electrode under various complex operating conditions.

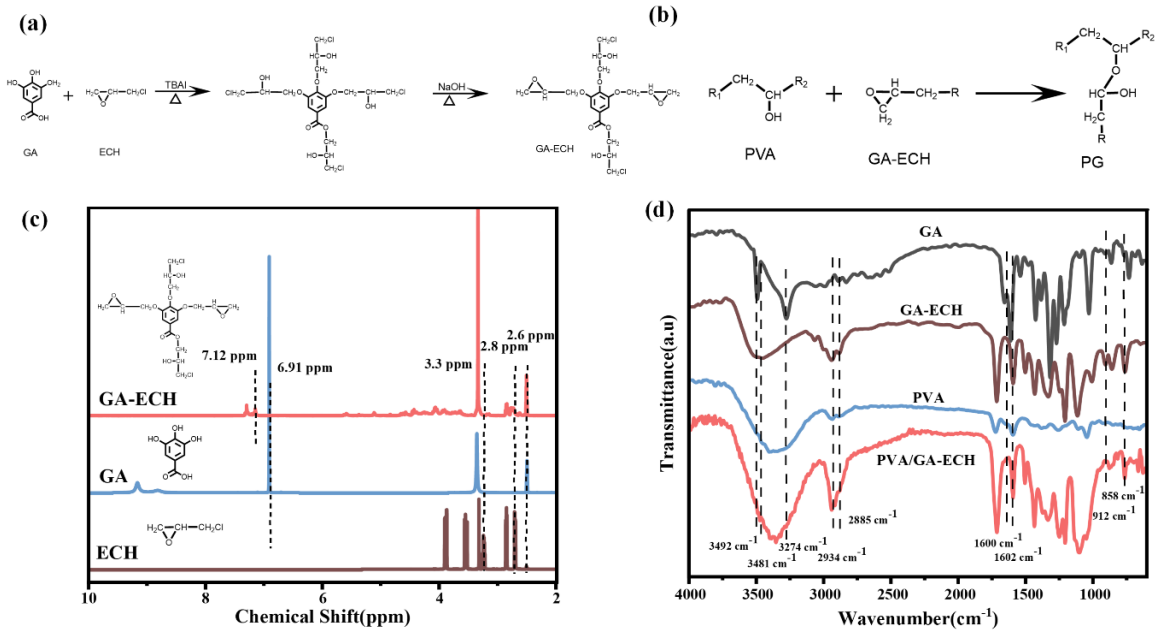

Figure 1. (**a**) The reaction scheme for epoxidation modification of GA, (**b**) The reaction equation for PVA with GA-ECH, (**c**) ^{1}H NMR spectra of GA, ECH and GA-ECH, (**d**) FTIR spectra of GA, PVA, GA-ECH, PVA/GA-ECH.

To further validate the mechanical properties of the aforementioned adhesives, hardness and modulus tests were conducted using a nanoindenter. Figure 2(b, c) indicate that PVA exhibits the lowest hardness and modulus, which can be attributed to its linear structure causing molecular chain slippage when silicon undergoes significant volume changes. This phenomenon poses a challenge to stabilizing the electrode structure during cycling, resulting in irreversible changes and a reduction in battery capacity. However, after cross-linking PVA with GA-ECH, the PG adhesive demonstrates excellent film-forming properties, accompanied by a significant increase in hardness and modulus. Consequently, the resulting dual-network structure is better equipped to handle the volume expansion of silicon during cycling, thereby maintaining a stable electrode structure and enhancing battery performance. These findings align with the results of the tensile testing analysis.

Adhesion strength is a critical property of adhesives, directly impacting the ability of electrodes to maintain electrical contact and structural integrity during cycling [38,39]. The significant volume expansion of silicon during cycling can lead to the loss of electrical

contact between the active material and the current collector, resulting in electrode structure collapse and a shortened battery lifespan. High adhesion strength enables close contact between silicon particles and copper foil, enhancing the stability of the electrode structure and improving cycling performance. Peel tests characterize the adhesion strength between silicon and copper foil. Figures 2(d, e) respectively show the peel test curves and average adhesion strength of silicon anodes prepared with different adhesives. The results indicate that the peel strength of the PG adhesive is higher than that of pure PVA (0.85 N), and it is highest (1.28 N) when the mass ratio of PVA to GA-ECH is 5:5. The improvement in peel strength is attributed to the introduction of GA-ECH. The molecular structure of GA-ECH contains hydroxyl and epoxy groups, which can not only form hydrogen bonds with PVA but also undergo ring-opening reactions to form covalent bonds. Additionally, a large number of active groups in the adhesive interact via hydrogen bonding with silicon particles and copper foil, effectively maintaining the integrity of the electrode structure and electrical contact.

The swelling performance of adhesives is closely related to their liquid absorption properties, with higher swelling aiding the migration of Li^+ in the electrode. As shown in Figure 2f, PVA has a low swelling rate, less than 10%, attributed to its high crystallinity. In contrast, PG55 exhibits the highest swelling rate at 19.62%, while PG73 and PG37 have swelling rates of 14.1% and 11.96%, respectively, significantly higher than PVA. This is because the introduction of GA-ECH disrupts the crystallinity of PVA, enlarging the gaps between molecular chains and increasing the swelling rate. It is worth noting that excessively high swelling rates can lead to a decrease in the adhesive's adhesion strength. However, the cross-linked network of PG prevents excessive swelling, keeping the swelling rate controlled between 10% and 20%, balancing adhesion strength and liquid absorption, thereby enhancing the battery's cycling performance.

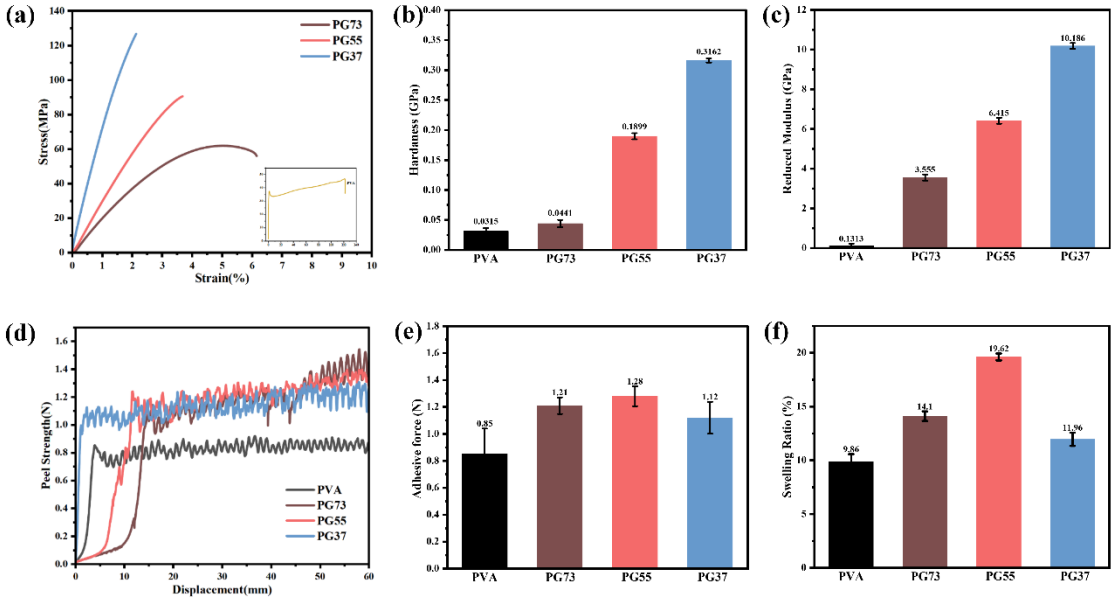

Figure 2. (**a**) The tensile curves of binder films, (**b**) hardness, (**c**) reduced modulus, (**d**) peel curves, (**e**) average adhesive force and (**f**) swelling ratio for silicon anodes prepared using PVA, PG73, PG55, and PG37 binders.

Before the preparation of the electrode, we used XRD (Figure S1) and SEM (Figure S2) to analyze the Si particles, indicating its crystallinity and particle size. To explore the impact of different binders on electrode cycling stability, galvanostatic charge/discharge tests were conducted on various half-cells within a voltage range of 0.005 to 1.5 V. Figure 3a outlines the initial charge-discharge cycles, where all cells were first activated at a current density of 210 mA g^{-1} before cycling at 420 mA g^{-1}. Table S1 summarizes the initial coulombic efficiency and initial charge-discharge capacities of the various electrodes. The first discharge capacities of the PVA electrode, PG73, PG55, and PG37 electrodes are 3753 mAh g^{-1}, 3759 mAh g^{-1}, 3875 mAh g^{-1}, and 3658 mAh g^{-1}, respectively, with corresponding first coulombic efficiencies of 80.33%, 85.82%, 88.92%, and 84.31%. The PVA electrode's lower first coulombic efficiency, at only 80.33%, is attributed to its high crystallinity (Figure S3), resulting in a dense electrode surface with low liquid absorption, which is unfavorable for lithium-ion transport. However, after cross-linking PVA with GA-ECH, the coulombic efficiency significantly improved, especially with a mass ratio of 5:5. This enhancement is due to the introduction of GA-ECH, which reduces the regularity and crystallinity of PVA molecular chains, increases electrolyte absorption, and promotes Li^+ transport. Moreover, the dual network structure formed by hydrogen bonds and covalent bonds effectively disperses the enormous stress caused by the volume expansion of silicon particles, maintains contact between the active materials and the current collector, stabilizes the SEI film on the electrode surface, reduces electrolyte consumption, and achieves higher coulombic efficiency.

The Si anodes, prepared with different adhesives, underwent cycling performance evaluation at a current density of 420 mA g^{-1}. Figures 3b and S4 provides a comprehensive overview of the cycling performance of various PG electrodes. Compared to the PVA electrode (1536 mAh g^{-1}), the PG electrodes exhibit significantly enhanced cycling stability. After 200 cycles, the remaining specific capacities of the PG73, PG55, and PG37 electrodes are 2289 mAh g^{-1}, 2480 mAh g^{-1}, and 2122 mAh g^{-1}, respectively. Among these, PG55 exhibits the best cycling stability. This improvement is attributed to the formation of a cross-linked network structure when PVA is combined with GA-ECH at a mass ratio of 5:5, enhancing both tensile and peel strength, effectively suppressing the excessive volume expansion of silicon particles, maintaining electrode structural stability, and extending electrode lifespan. Conversely, at a mass ratio of 7:3, the fewer covalent bonds formed are less effective in suppressing the excessive volume expansion of silicon, resulting in silicon particle fracturing, excessive electrolyte consumption, and the formation of a thicker SEI film, leading to reduced residual battery capacity. Meanwhile, at a ratio of 3:7, excessive GA-ECH leads to a significant number of remaining epoxy groups on the molecular chains, which undergo aging during extended cycling, significantly reducing the mechanical properties of the PG37 adhesive and weakening its ability to inhibit silicon particles, ultimately resulting in poorer cycling performance. To further verify the stabilizing effect of the PG binder on the anode at higher current densities, we conducted cycling performance tests at a current density of 840 mA g^{-1}. As shown in Figures 3c and S5, after 200 cycles, the remaining specific capacities of the PG73, PG55, and PG37 electrodes were 1597 mAh g^{-1},

1822 mAh g^{-1}, and 1403 mAh g^{-1}, respectively. Additionally, we compared the performance of PG binders with that of general binders such as CMC [40] and PAA [41], as reported in the literature. Specifically, CMC achieved a capacity of 1178 mAh g^{-1} after 100 cycles at a current density of 400 mAh g^{-1}, while PAA only reached 1046 mAh g^{-1} after 150 cycles at a current density of 300 mA g^{-1}. In comparison, the electrode prepared with the PG55 binder in this work exhibited superior cycling stability.

Additionally, rate performance tests were conducted on different electrodes at current densities of 210 mA g^{-1}, 420 mA g^{-1}, 840 mA g^{-1}, and 2100 mA g^{-1} within the voltage range of 0.005–1.5 V. As shown in Figure 3d, the PVA and PG73 electrodes exhibit low cycling capacity and rapid decay at high current densities. This is because PG73 contains the highest amount of PVA components and has the least degree of cross-linking, resulting in mechanical properties similar to those of the PVA binder. Consequently, at high currents, during the rapid intercalation/deintercalation of lithium ions, neither PG73 nor the PVA binder can effectively suppress the volume expansion of the Si anode, resulting in extremely low discharge capacities. In contrast, benefiting from superior mechanical properties and a more robust dual cross-linking structure, the PG55 and PG37 binders can stabilize the electrode structure. Both exhibit higher cycling-specific capacities at high current densities and when the current density returns to 420 mA g^{-1}, the specific capacity also returns to its initial value, indicating a high reversible capacity. This further underscores the beneficial role of hydrogen bonds and covalent bonds in the three-dimensional network in maintaining electrode structural stability and enhancing battery cycling performance.

Cyclic voltammetry (CV) curves serve as indicators of the lithium deintercalation process during electrode cycling. In this study, the PG55 electrodes underwent three CV scans within the 0–1.5 V voltage range at a scan rate of 0.1 mV s^{-1}. As illustrated in Figure 3e, the reduction peaks at 0.20 V and 0.01 V are associated with the formation of $Li_{12}Si_7$ and $Li_{15}Si_4$ alloy phases during discharge, respectively. Crystalline silicon undergoes a two-step phase transition to form lithium silicide (Li_xSi) alloys. Conversely, the peaks at 0.37 V and 0.52 V correspond to lithium extraction during battery charging, where lithium silicide de-alloys form amorphous silicon. With the scan progression, these peaks increase in magnitude, indicating thorough lithium deintercalation processes within the electrode that become progressively activated. Furthermore, Figure S6 illustrates the cyclic voltammograms of pure PG55 adhesive within the working voltage range of 0–1.5 V. It is evident that after scanning at a voltage scan rate of 0.1 mV s^{-1}, no distinct redox peaks are observed. This observation suggests excellent electrochemical stability of the PG55 binder within the working voltage range of silicon anodes, thus meeting the requirements for the binders of silicon anodes.

The impact of different binders on the electrochemical kinetics of the Si anode was further investigated using electrochemical impedance spectroscopy (EIS). Before cycling, all electrodes exhibited similar interface impedances (the fitting circuit is shown in Figure S7), as illustrated in Figure S8. However, after 100 cycles at a current density of 420 mA g^{-1} (Figure 3f, the fitting circuit is shown in Figure S9), all PG electrodes showed lower interface impedances compared to the PVA electrode. This improvement is attributed to the

excellent mechanical properties and unique dual-crosslinking structure of PG binders, which effectively mitigate the volume expansion of the Si anode during cycling, ensuring the integrity of the electrode structure and the stability of the SEI film.

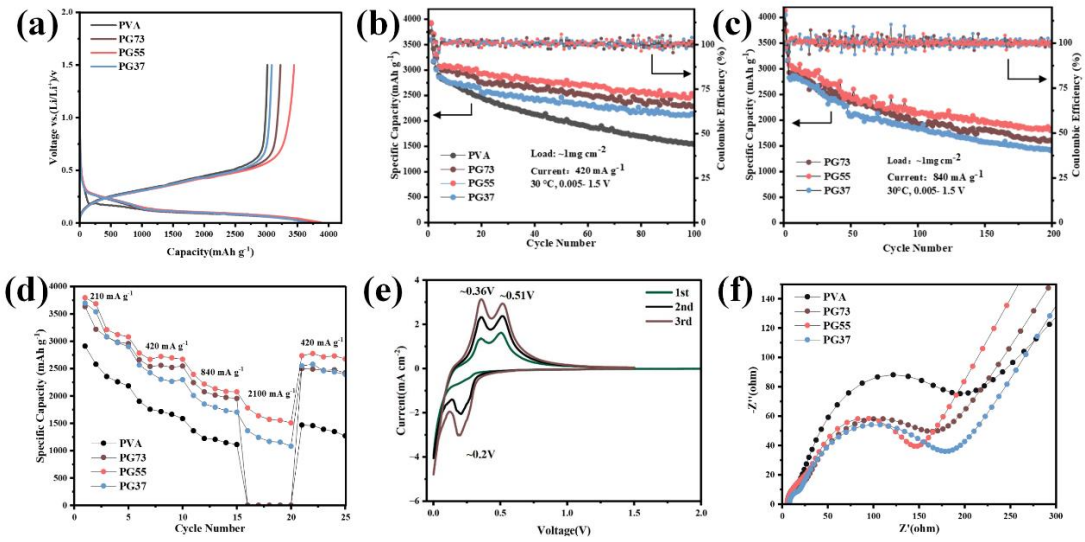

Figure 3. (**a**) Details of initial charge-discharge for each anode, (**b**) cycling behavior of PVA, PG73, PG55, and PG37 electrodes at a current density of 420 mA g^{-1}, (**c**) cycling behavior of PG73, PG55, and PG37 electrodes at a current density of 840 mA g^{-1}, (**d**) rate performance plots of PVA, PG73, PG55, and PG37 electrodes, (**e**) cyclic voltammetry curve of PG55 electrode, (**f**) electrochemical impedance spectroscopy of PVA, PG73, PG55, and PG37 electrodes after 100 cycles at 420 mA g^{-1} current density.

SEM images of electrodes prepared with different binders before and after cycling are presented in Figure 4. Figure 4a illustrates the highly dense surface of the PVA electrode, attributed to its high crystallinity, resulting in a low liquid absorption rate in swelling tests. This density impedes the access of lithium ions to the silicon surface, leading to lower initial Coulombic efficiency and subpar cycling performance. Conversely, after cross-linking PVA with modified GA-ECH, the dense crystallinity of PVA is disrupted, creating a porous structure on the surface of the PG electrode (Figure 4c, e, g). This porous morphology facilitates lithium-ion transport, thus improving initial Coulombic efficiency and cycling performance. After 100 cycles at a current density of 420 mA g^{-1}, the PVA electrode surface exhibits numerous large cracks, attributed to the linear structure of polyvinyl alcohol being ineffective in mitigating the volume expansion of silicon particles during cycling. This results in substantial changes in the electrode surface structure, increased electrolyte consumption, reduced lithium ion content, and ultimately, degraded cycling performance. In contrast, the surface of the PG electrode remains predominantly intact without significant cracks, indicating that the binder's high-strength dual-network structure effectively suppresses the volume expansion of silicon particles, preserves the integrity of the electrode structure, and promotes the formation of a stable SEI film. This mitigates further electrolyte consumption, thereby enhancing the cycling lifespan of lithium-ion batteries.

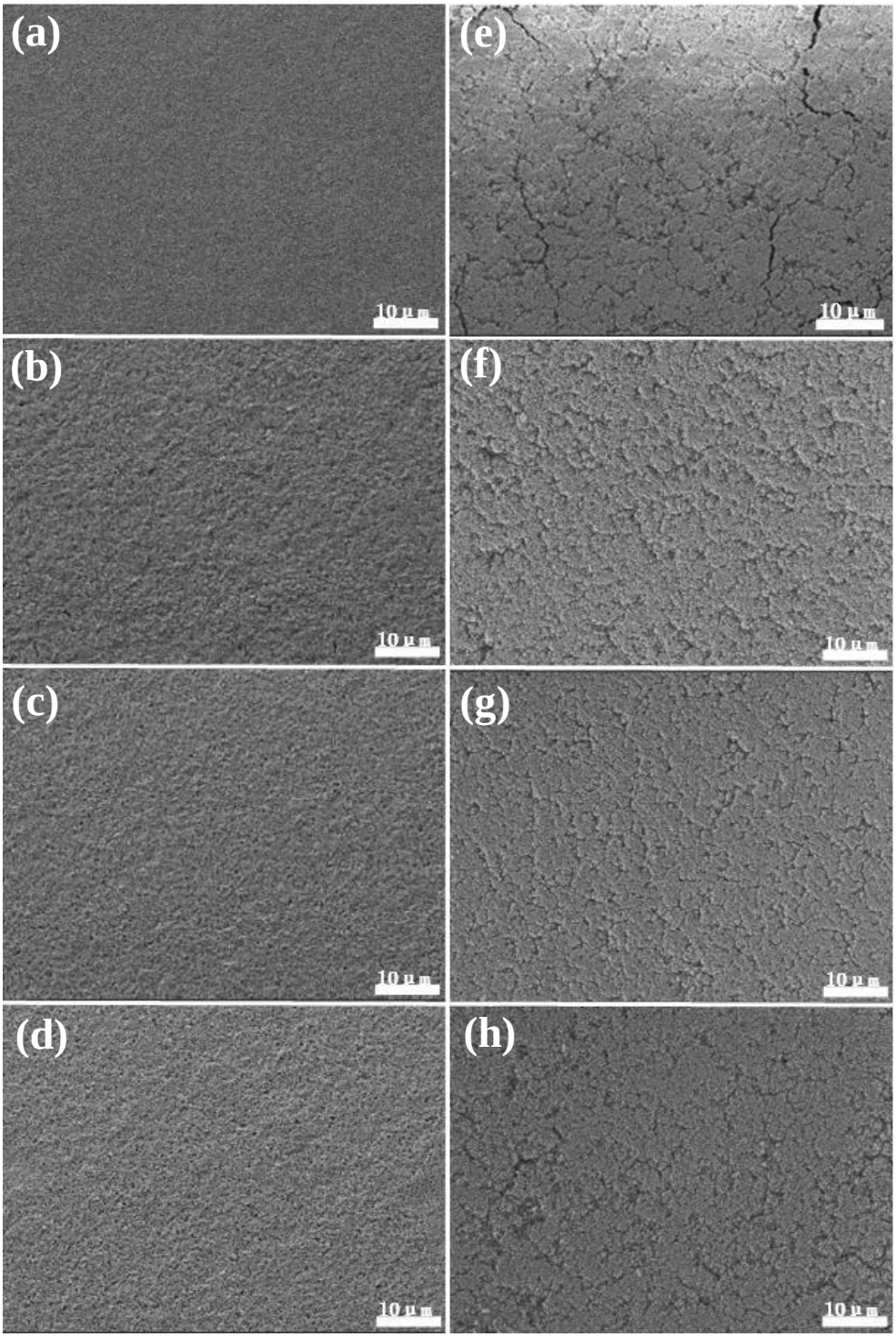

Figure 4. Surface SEM images of different electrodes before and after cycling. (**a**) PVA@Si, (**b**) PG73@Si, (**c**) PG55@Si, (**d**) PG37@Si electrodes before cycling, (**e**) PVA@Si, (**f**) PG73@Si, (**g**) PG55@Si, (**h**) PG37@Si electrodes after cycling 100 times at a current density of 420 mA g^{-1}.

4. Conclusion

In this study, GA was modified with ECH, successfully grafting epoxy groups onto its molecular structure. Subsequently, these groups cross-linked with hydroxyl groups in PVA, forming hydrogen bonds between unreacted polar groups, while the presence of benzene rings endowed the binder with high mechanical strength. This resulted in the preparation of a binder with a robust three-dimensional dual network structure of hydrogen and covalent bonds. Tensile and nanoindentation tests demonstrated that the cross-linked binder exhibited high mechanical strength, effectively mitigating significant volume expansion in silicon. Peel tests indicated that the PG binder possessed strong adhesion, ensuring close contact between active materials and current collectors, thereby enhancing battery cycling performance. Constant current charge-discharge tests revealed that the PG55 electrode exhibited superior cycling performance, with an initial Coulombic efficiency as high as 88.92% and a specific capacity of 1822 mAh g^{-1} after 200 cycles at a current density of approximately 840 mA g^{-1} and a mass loading around 1.0 mg cm^{-2}. SEM analysis further confirmed that the PG55 electrode maintained a more intact electrode structure. In conclusion, the experimental results demonstrate that the high-strength three-dimensional dual network binder can effectively mitigate silicon volume expansion to maintain electrode structural integrity, thereby exhibiting excellent cycling performance in batteries.

Supplementary data

The authors confirm that the supplementary data are available within this article. Table S1. Experimental results of electrochemical characterization; Figure S1. XRD curve of Si particles; Figure S2. The SEM image of Si particles in this work; Figure S3. XRD diffraction pattern of PVA; Figure S4. cycling results of PVA, PG73, PG55, and PG37 electrodes at a current density of 420 mA g^{-1}; Figure S5. cycling results of PG73, PG55, and PG37 electrodes at a current density of 840 mA g^{-1}; Figure S6. The CV curve of PG55 scanned at a voltage scan rate of 0.1 mV s^{-1} within the range of 0–1.5V; Figure S7. EIS analogue equivalent circuit diagram of after the cycle; Figure S8. The electrochemical impedance spectra of each electrode before cycling; Figure S9. EIS analogue equivalent circuit diagram of before the cycle.

Acknowledgement

This work was supported by the Shandong Province Taishan Scholars Program (project No.: tsqn202312206); Shandong Province Youth Entrepreneurship Technology Support Program for Higher Education Institutions (project No.: 2023KJ308).

Conflicts of interests

The authors declare no conflicts of interest.

Authors' contribution

Conceptualization and design: Junchao Sun and Jing Jiang; methodology: Junchao Sun and Jing Jiang; software and validation: Zhengshuai Xu and Lintianfang Su; formal analysis: Hongwei Pan; investigation and data curation: Zhengshuai Xu, Lintianfang Su; resources: Yongyin Cui, Hongwei Pan and Lan Cao; writing—original draft preparation: Junchao Sun and Jing Jiang; writing—review and editing: Hongwei Pan; supervision: Yongyin Cui, Hongwei Pan and Lan Cao; project administration: Yongyin Cui, Hongwei Pan and Lan Cao; funding acquisition: Lan Cao. All authors have read and agreed to the published version of the manuscript.

References

[1] Ge M, Cao C, Biesold GM, Sewell CD, Hao SM, *et al.* Recent Advances in Silicon-Based Electrodes: From Fundamental Research Toward Practical Applications. *Adv. Mater.* 2021, 33(16):2004577.

[2] Manthiram A. A Reflection on Lithium-Ion Battery Cathode Chemistry. *Nat. Commun.* 2020, 11(1):1550.

[3] Lao X, Yang M, Chen J, Zhang LY, Guo P. The Ethanol Oxidation Reaction on Bimetallic Pdxag1-X Nanosheets in Alkaline Media and Their Mechanism Study. *Electrochim. Acta* 2021, 374:137912.

[4] Xu R, Wei R, Hu X, Li Y, Wang L, *et al.* A Strategy and Detailed Explanations to the Composites of Si/Mwcnts for Lithium Storage. *Carbon* 2021, 171:265–275.

[5] Wu J, Zhang X, Ju Z, Wang L, Hui Z, *et al.* From Fundamental Understanding to Engineering Design of High-Performance Thick Electrodes for Scalable Energy-Storage Systems. *Adv. Mater.* 2021, 33(26):2101275.

[6] Meng J, Xu H, Ma Q, Li Z, Xu L, *et al.* Precursor Pre-Oxidation Enables Highly Exposed Plane for High-Rate Li-Rich Layered Oxide Cathode Materials. *Electrochim. Acta* 2019, 309:326–338.

[7] Ko M, Chae S, Ma J, Kim N, Lee HW, *et al.* Scalable Synthesis of Silicon-Nanolayer-Embedded Graphite for High-Energy Lithium-Ion Batteries. *Nat. Energy* 2016, 1(9):1–8.

[8] Chen H, Yang Y, Boyle DT, Jeong YK, Xu R, *et al.* Free-Standing Ultrathin Lithium Metal–Graphene Oxide Host Foils with Controllable Thickness for Lithium Batteries. *Nat. Energy* 2021, 6(8):790–798.

[9] Bruce PG, Scrosati B, Tarascon JM. Nanomaterials for Rechargeable Lithium Batteries. *Angew. Chem. Int. Ed.* 2008, 47(16):2930–2946.

[10] McDowell MT, Lee SW, Nix WD, Cui Y. 25th Anniversary Article: Understanding the Lithiation of Silicon and Other Alloying Anodes for Lithium-Ion Batteries. *Adv. Mater.* 2013, 25(36):4966–4985.

[11] Kim H, Seo M, Park MH, Cho J. A Critical Size of Silicon Nano-Anodes for Lithium Rechargeable Batteries. *Angew. Chem. Int. Ed.* 2010, 49(12):2146–2149.

[12] Zhang L, Wang C, Dou Y, Cheng N, Cui D, *et al.* A Yolk–Shell Structured Silicon Anode with Superior Conductivity and High Tap Density for Full Lithium-Ion Batteries. *Angew. Chem. Int. Ed.* 2019, 58(26), 8824–8828.

[13] Han Y, Lin N, Xu T, Li T, Tian J, *et al.* An Amorphous Si Material with a Sponge-Like Structure as an Anode for Li-Ion and Na-Ion Batteries. Nanoscale 2018, 10(7):3153–3158.

[14] Song H, Wang S, Song X, Yang H, Du G, *et al.* A Bottom-up Synthetic Hierarchical Buffer Structure of Copper Silicon Nanowire Hybrids as Ultra-Stable and High-Rate Lithium-Ion Battery Anodes. *J. Mater. Chem. A* 2018, 6(17):7877–7886.

[15] An W, Gao B, Mei S, Xiang B, Fu J, *et al.* Scalable Synthesis of Ant-Nest-Like Bulk Porous Silicon for High-Performance Lithium-Ion Battery Anodes. *Nat. Commun.* 2019, 10(1):1447.

[16] Yang J, Wang Y, Li W, Wang L, Fan Y, *et al.* Amorphous Tio2 Shells: A Vital Elastic Buffering Layer on Silicon Nanoparticles for High‐Performance and Safe Lithium Storage. *Adv. Mater.* 2017, 29(48):1700523.

[17] Saint J, Morcrette M, Larcher D, Laffont L, Beattie S, *et al.* Towards a Fundamental Understanding of the Improved Electrochemical Performance of Silicon–Carbon Composites. *Adv. Funct. Mater.* 2007, 17(11):1765–1774.

[18] Kwon T, Choi JW, Coskun A. The Emerging Era of Supramolecular Polymeric Binders in Silicon Anodes. *Chem. Soc. Rev.* 47(6):2145–2164.

[19] Choi JY, Lee DJ, Lee YM, Lee YG, Kim KM, *et al.* Silicon Nanofibrils on a Flexible Current Collector for Bendable Lithium‐Ion Battery Anodes. *Adv. Funct. Mater.* 2012, 23(17):2108–2114.

[20] Chen H, Wu Z, Su Z, Chen S, Yan C, *et al.* A Mechanically Robust Self-Healing Binder for Silicon Anode in Lithium Ion Batteries. *Nano Energy* 2021, 81:105654.

[21] Liu J, Zhang Q, Zhang T, Li JT, Huang L, *et al.* A Robust Ion-Conductive Biopolymer as a Binder for Si Anodes of Lithium‐Ion Batteries. *Adv. Funct. Mater.* 2015, 25(23):3599–3605.

[22] Li J, Zhang G, Yang Y, Yao D, Lei Z, *et al.* Glycinamide Modified Polyacrylic Acid as High-Performance Binder for Silicon Anodes in Lithium-Ion Batteries. *J. Power Sources* 2018, 406:102–109.

[23] Tian M, Chen X, Sun S, Yang D, Wu P. A Bioinspired High-Modulus Mineral Hydrogel Binder for Improving the Cycling Stability of Microsized Silicon Particle-Based Lithium-Ion Battery. *Nano Res.* 2019, 12:1121–1127.

[24] Zheng Z, Gao H, Ke C, Li M, Cheng Y, *et al.* Constructing Robust Cross-Linked Binder Networks for Silicon Anodes with Improved Lithium Storage Performance. *ACS Appl. Mater. Interfaces* 2021, 13(45):53818–53828.

[25] Wang Z, Huang T, Liu Z, Yu A. Dopamine-Modified Carboxymethyl Cellulose as an Improved Aqueous Binder for Silicon Anodes in Lithium-Ion Batteries. *Electrochim. Acta* 2021, 389:138806.

[26] Zhao J, Wei D, Wang J, Yang K, Wang Z, *et al.* Inorganic Crosslinked Supramolecular Binder with Fast Self-Healing for High Performance Silicon Based Anodes in Lithium-Ion Batteries. *J. Colloid Interface Sci.* 2022, 625:373–382.

[27] Li J, Wang Y, Xie X, Kong Z, Tong Y, *et al.* A Novel Multi-Functional Binder Based on Double Dynamic Bonds for Silicon Anode of Lithium-Ion Batteries. *Electrochim. Acta* 2022, 425:140620.

[28] Guo R, Zhang S, Ying H, Yang W, Wang J, *et al.* Preparation of an Amorphous Cross-Linked Binder for Silicon Anodes. *ChemSusChem* 2019, 12(21):4838–4845.

[29] Koo B, Kim H, Cho Y, Lee KT, Choi NS, *et al.* A Highly Cross-Linked Polymeric Binder for High‐Performance Silicon Negative Electrodes in Lithium Ion Batteries. *Angew. Chem. Int. Ed.* 2012, 35(124):8892–8897.

[30] Jeong YK, Kwon T, Lee I, Kim TS, Coskun A, *et al.* Hyperbranched B-Cyclodextrin Polymer as an Effective Multidimensional Binder for Silicon Anodes in Lithium Rechargeable Batteries. *Nano Lett.* 2014, 14(2):864–870.

[31] Pan H, Xu Z, Wei Z, Liu X, Xu M, *et al.* Synergistic Double Cross-Linked Dynamic Network of Epoxidized Natural Rubber/Glycinamide Modified Polyacrylic Acid for Silicon Anode in Lithium Ion Battery: High Peel Strength and Super Cycle Stability. *ACS Appl. Mater. Interfaces* 2022, 14(29):33315–33327.

[32] Zheng M, Wang C, Xu Y, Li K, Liu D. A Water-Soluble Binary Conductive Binder for Si Anode Lithium Ion Battery. *Electrochim. Acta* 2019, 305:555–562.

[33] Jin B, Lai T, Manthiram A. High-Mass-Loading Anode-Free Lithium–Sulfur Batteries Enabled by a Binary Binder with Fast Lithium-Ion Transport. *ACS Energy Lett.* 2023, 8(9):3767–3774.

[34] Jin B, Wang D, Song L, Cai Y, Ali A, *et al.* Biomass-Derived Fluorinated Corn Starch Emulsion as Binder for Silicon and Silicon Oxide Based Anodes in Lithium-Ion Batteries. *Electrochim. Acta* 2021, 365:137359.

[35] Jin B, Wang D, Zhu J, Guo H, Hou Y, *et al.* A Self‐Healable Polyelectrolyte Binder for Highly Stabilized Sulfur, Silicon, and Silicon Oxides Electrodes. *Adv. Funct. Mater.* 2021, 31(41):2104433.

[36] Li Z, Ji J, Wu Q, Wei D, Li S, *et al.* A New Battery Process Technology Inspired by Partially Carbonized Polymer Binders. *Nano Energy* 2020, 67:104234.

[37] Chen H, Ling M, Hencz L, Ling HY, Li G, *et al.* Exploring Chemical, Mechanical, and Electrical Functionalities of Binders for Advanced Energy-Storage Devices. *Chem. Rev.* 2018, 118(18):8936–8982.

[38] Liu T, Chu Q, Yan C, Zhang S, Lin Z, *et al.* Interweaving 3d Network Binder for High-Areal-Capacity Si Anode through Combined Hard and Soft Polymers. *Adv. Energy Mater.* 2018, 9(3):1802645.

[39] Jiang X, Cui X, Duncan AJE, Li L, Hughes RP, *et al.* Topochemical Synthesis of Single-Crystalline Hydrogen-Bonded Cross-Linked Organic Frameworks and Their Guest-Induced Elastic Expansion. *J. Am. Chem. Soc.* 2019, 141(27):10915–10923.

[40] Song J, Zhou M, Yi R, Xu T, Gordin M. L, *et al.* Interpenetrated Gel Polymer Binder for High-Performance Silicon Anodes in Lithium-Ion Batteries. *Adv. Funct. Mater.* 2014, 24(37):5904–5910.

[41] Chen X, Wang R, Zhang X, Yang Y, Sun W, *et al.* Remarkably Improved Cycling Stability of Commercial Micron-Sized Silicon Enabled by a Novel Organic/Inorganic Hybrid Binder. *J. Power Sources* 2024, 607:234595.